


The Modulation of Galactic Cosmic Ray Intensity in the Outer Heliosphere

Yurii Fedorov¹ · Milan Stehlik² 

Received: 3 October 2016 / Accepted: 11 July 2017 / Published online: 16 August 2017
© Springer Science+Business Media B.V. 2017

Abstract *Voyager* 1 and 2 observations could improve a model of the heliosphere that includes the supersonic solar wind and heliosheath as far as local interstellar space. This enables us to construct a simple model of the propagation of galactic cosmic-ray particles (GCR) in the heliosphere and its magnetic fields. Solutions of the cosmic-ray transport equation in an spherical force-field approximation (Gleeson and Urch in *Astrophys. Space Sci.* **25**:387, 1973) are generalized, and then they are modified in a second-order approximation assuming a small GCR streaming (GCR anisotropy) as a smallness parameter. GCR reacceleration on shock waves is not considered in our model. This idealized approach still yields additional insight into the process of GCR distribution in the real heliosphere. The energy and spatial distribution of the GCR intensity is investigated in separate regions of the heliosphere. The GCR energy streaming is estimated, and the anisotropy in the GCR angular distribution is computed for particle kinetic energies from 100 MeV up to 10 GeV.

Keywords Cosmic rays, galactic · Energetic particles, propagation

1. Introduction

The galactic cosmic-ray (GCR) intensity in the heliosphere (HS) is lower than the intensity in the local interstellar space (IS), which is due to the interaction of high-energy charged particles with the solar-wind (SW) plasma. Electromagnetic fields, which are carried by moving interplanetary plasma, change the GCR energy spectrum and also cause an increase in anisotropy in the particle angular distribution. During the past few decades, unique information about the structure of the heliosphere, interplanetary magnetic fields, and high-energy particles that propagate in the fields has been obtained using

✉ M. Stehlik
stehlik@saske.sk

Y. Fedorov
fedorov@mao.kiev.ua

¹ Main Astronomical Observatory, National Academy of Sciences of Ukraine, Kiev, Ukraine

² Institute of Experimental Physics, Slovak Academy of Sciences, Košice, Slovakia

in-situ observations together with theoretical calculations (Florinski and Pogorelov, 2009; Scherer *et al.*, 2011; Potgieter, 2013; Richardson and Burlaga, 2013; Manuel, Ferreira, and Potgieter, 2014). The supersonic SW propagates to heliocentric distances 80–95 AU, *i.e.* to the heliospheric shock wave (termination shock). *Voyager 1* left the SW region and entered the heliosheath at a distance of 94 AU from the Sun (Burlaga *et al.*, 2005; Decker *et al.*, 2005; Stone *et al.*, 2005), and *Voyager 2* passed above the shock wave at a distance of 84 AU (Burlaga *et al.*, 2008; Decker *et al.*, 2008; Richardson *et al.*, 2008; Stone *et al.*, 2008). The SW velocity is radial, and it weakly depends on the heliocentric distance.

The termination shock (TS) separates the SW from the heliosheath – the region of space that spreads out to the heliopause. The SW velocity decreases by about a factor of three at the TS, and then the SW velocity in the heliosheath continuously decreases with distance from the Sun (Burlaga *et al.*, 2009; Richardson and Stone, 2009; Richardson and Burlaga, 2013).

In the investigation of CR propagation in the HS, authors frequently use the approximation that the hydrodynamic velocity of SW plasma in the heliosheath decreases with heliocentric distance (Richardson and Burlaga, 2013; Manuel, Ferreira, and Potgieter, 2014; Kota and Jokipii, 2014; Fedorov, 2014, 2015). The influence of the SW velocity spatial dependence in the heliosheath on the spatial-energy distribution of the CR has been examined by Langner *et al.* (2006a, 2006b). They demonstrated that various spatial profiles of the SW velocity in the heliosheath do not lead to noticeable influence at the CR intensity in the inner HS. Nevertheless, the GCR distribution in the heliosheath strongly depends on the spatial profile of the hydrodynamic plasma velocity.

In 2012, *Voyager 1* crossed the heliopause at a distance of 122 AU from the Sun; then it left the boundary of the HS and began to measure physical characteristics of the local IS including the CR intensity (Burlaga, Ness, and Stone, 2013; Krimigis *et al.*, 2013; Stone *et al.*, 2013; Webber and McDonald, 2013; Kota and Jokipii, 2014; Strauss and Fichtner, 2014). The data made it possible to determine the proton energy spectrum down to 10^6 eV in the local IS (Potgieter and Strauss, 2013; Webber and McDonald, 2013; Potgieter, 2014; Bisschoff and Potgieter, 2015; Cummings *et al.*, 2015). According to the *Voyager 1* observations, the HS is surrounded by a region in which the propagation of high-energy particles is hindered. Near the heliopause, an increase in GCR intensity has been detected that was caused by a substantial value of the particle density radial gradient (Krimigis *et al.*, 2013; Stone *et al.*, 2013; Kota and Jokipii, 2014). At greater distances from the HS, the GCR intensity detected by *Voyager 1* remains at a constant level that corresponds to the high-energy particle density in the local IS (Kota and Jokipii, 2014).

The GCR transport in the outer HS was also investigated by numerical analysis of the transport equation under various assumptions about the HS structure (see, *e.g.* Florinski and Pogorelov, 2009; Scherer *et al.*, 2011; Herbst *et al.*, 2012; Kota and Jokipii, 2014; Guo and Florinski, 2014; Strauss and Fichtner, 2014; Zhang, Luo, and Pogorelov, 2015).

It is well known that the GCR streaming is represented by the superposition of a particle-diffusion flux directed into the HS and convection directed out from the Sun (Dolginov and Toptygin, 1966; Gleeson and Axford, 1968). As a result, the GCR streaming becomes considerably weaker than either of its components. The well-known “force-field” approximation of Gleeson and Axford (1968) and Gleeson and Urch (1973) (see also Moraal, 2013) is based on setting equal to zero the particle streaming of the given momentum, and on solving of the obtained first-order partial differential equation. This approach was advanced by Shakhov and Kolesnik (2006), who developed an analytical iteration procedure using the particle streaming as a smallness parameter. Note that according to Caballero-Lopez and

Moraal (2004), the force-field equation approximates a one-dimensional spherical steady-state transport equation better in the inner HS and in the outer HS, the convection–diffusion approximation is better than the force-field approximation (Moraal, 2013). Thus a development of the force-field approximation using further iterations appeared to be useful.

In the present article the force-field approximation is applied as the first step for all regions including the outer HS. The generalized first-order solution obtained is then in the second step modified using the analytical iteration procedure of Shakhov and Kolesnik (2006). Note that in correspondence with ground-level observations at Earth as well as data of probes in space, the anisotropy in the GCR angular distribution has a low value (considerably lower than unity) for a large range of particle energies (Schlickeiser, 2002; Dorman, 2006; Potgieter, 2013).

This method of the approximate solution of the CR transport equation is here applied for the spherical model that includes the supersonic SW, the heliosheath, and the IS. The SW velocity in the heliosheath decreases with some given power of the heliocentric distance, and continuity conditions for the CR density and particle streaming are satisfied at the TS as well as at the heliopause (a surface bounding the HS). The GCR energy distribution is assumed to be fixed in the IS at distances considerably exceeding the size of the HS. The GCR reacceleration on shock waves is not considered in our model. We analyze the spatial GCR distribution and its energy spectra.

2. The Advanced Force-Field Approximation

Here we investigate the generalized force-field model for the whole extended region of the HS, which is assumed to be spherical. Let us assume that the SW is radial and constant in the inner HS that is bounded by the spherical TS, which is located at a distance r_0 from the Sun. Then the SW velocity is $u(r) = u_0 = \text{const.}$ for $r < r_0$. We place the medium compression coefficient σ at the TS $\sigma \approx 3$ by analogy with Richardson and Burlaga (2013) and Manuel, Ferreira, and Potgieter (2014), and the shock then is $u(r_0) = u_0/\sigma$. The spherical heliopause, which separates the solar and interstellar plasma, is located at r_1 ; thus, the heliosheath is stretched in the spatial region $\{r_0, r_1\}$, where $u(r)$ is inversely proportional to the heliocentric distance to the power α ($\alpha \geq 2$):

$$u(r) = \frac{u_0}{\sigma \varrho^\alpha}, \quad \varrho = \frac{r}{r_0}, \quad (1 < \varrho < \varrho_1). \quad (1)$$

Here we introduce a dimensionless heliocentric distance ϱ ; consequently, $\varrho = 1$ at the TS and $\varrho = \varrho_1 \equiv r_1/r_0$ at the outer boundary of the HS. We neglect the movement of plasma behind the heliopause, $u = 0$ for $\varrho > \varrho_1$. In the current model, the TS and the heliopause are located at $r_0 = 80$ AU and $r_1 = 120$ AU, respectively; thus, $\varrho_0 = 1$, $\varrho_1 = 1.5$.

The CR transport equation for the particle density $[N(r, p)]$ in the spherical symmetry considered reads (Parker, 1965; Dolginov and Topygin, 1966; Gleeson and Axford, 1968)

$$\frac{1}{r^2} \frac{\partial}{\partial r} r^2 \kappa \frac{\partial N}{\partial r} - u(r) \frac{\partial N}{\partial r} + \frac{p}{3} \frac{\partial N}{\partial p} \frac{1}{r^2} \frac{\partial}{\partial r} r^2 u(r) = 0, \quad (2)$$

where κ is the diffusion coefficient. Correspondingly, the particle streaming consists of two components, the diffusion and convective particles,

$$j(r, p) = -\kappa \frac{\partial N}{\partial r} - \frac{u(r)}{3} p \frac{\partial N}{\partial p}. \quad (3)$$

In the following we use a dimensionless particle momentum $\eta = p/mc$, where m is the proton rest mass, and c is the speed of light.

GCR Density in the Heliosheath Let us investigate the GCR spatial-energy distribution in the heliosheath ($1 < \varrho < \varrho_1$), where the SW velocity is defined in Equation 1, and the streaming in Equation 3 in terms of the dimensionless variables ϱ, η is

$$j(\varrho, \eta) = -\frac{u_0}{\sigma} \left\{ \frac{1}{\mu_1(\eta)} \frac{\partial N}{\partial \varrho} + \frac{\eta}{3\varrho^\alpha} \frac{\partial N}{\partial \eta} \right\}. \tag{4}$$

The introduced CR modulation parameter $\mu = ur/\kappa$ in the heliosheath is equal to

$$\mu_1(\eta) = \frac{u_0 r_0}{\sigma \kappa_1(\eta)}, \tag{5}$$

where $\kappa_1(\eta)$ is the CR diffusion coefficient in the heliosheath. We assume a power-law dependence of κ_1 on the particle momentum [$\kappa_1(\eta) = \kappa_{01}\eta^\lambda$] where κ_{01} is the diffusion coefficient of particles with momentum $p = mc$ ($\eta = 1$). The value $\eta = 1$ corresponds to a proton kinetic energy of 389 MeV. Thus the parameter $\mu_1(\eta) = \mu_{01}\eta^{-\lambda}$, where $\mu_{01} = u_0 r_0 / \sigma \kappa_{01}$.

In what follows, we apply an approximate method of solving the CR transport equation, which uses a weak anisotropy in the particle angular distribution as a smallness parameter (Gleeson and Axford, 1968; Urch and Gleeson, 1972; Gleeson and Urch, 1973; Shakhov and Kolesnik, 2006). Initially, we assume the GCR distribution function to be isotropic and the particle streaming (Equation 3) to be zero at each point in space. Thus in the given approximation, the GCR density outside the HS does not depend on the spatial coordinates, i.e. $N(\varrho, \eta) \equiv N_0(\eta)$ for $\varrho > \varrho_1$, where $N_0(\eta)$ describes the GCR energy distribution in the local IS.

The condition of zero CR streaming (Equation 4) with the continuity condition

$$N|_{\varrho=\varrho_1} = N_0(\eta)$$

leads to a first-order partial differential equation. As a result, the GCR density in the heliosheath $1 < \varrho < \varrho_1$ is

$$N(\varrho, \eta) = N_0(\xi_1), \tag{6}$$

$$\xi_1 = \left[\eta^\lambda + \frac{\mu_{01}\lambda}{3(\alpha - 1)} (\varrho^{1-\alpha} - \varrho_1^{1-\alpha}) \right]^{1/\lambda}. \tag{7}$$

GCR Density in the Solar Wind Now we investigate the GCR spatial-energy distribution in the SW. In this HS region ($\varrho < 1$), we take the SW velocity to be constant, thus the streaming (Equation 3) is

$$j(\varrho, \eta) = -u_0 \left\{ \frac{1}{\mu(\eta)} \frac{\partial N}{\partial \varrho} + \frac{\eta}{3} \frac{\partial N}{\partial \eta} \right\}, \tag{8}$$

$$\mu(\eta) = \frac{u_0 r_0}{\kappa(\eta)}. \tag{9}$$

Assuming again a power-law dependence of κ , $\kappa(\eta) = \kappa_0\eta^\lambda$, where $\kappa_0 = \kappa|_{\eta=1}$, the modulation parameter becomes $\mu(\eta) = \mu_0\eta^{-\lambda}$, $\mu_0 = u_0 r_0 / \kappa_0$. Setting the streaming (Equation 8) to zero, we obtain the GCR density in the SW ($\varrho < 1$),

$$N(\varrho, \eta) = N_0(\xi), \tag{10}$$

$$\xi = \left[\eta^\lambda + \frac{\mu_0 \lambda}{3} (1 - \varrho) + \frac{\mu_{01} \lambda}{3(\alpha - 1)} (1 - \varrho_1^{1-\alpha}) \right]^{1/\lambda}. \quad (11)$$

Note that with our choice of variables ξ (Equation 11) and ξ_1 (Equation 7), the GCR density (Equations 10, 6) satisfies the continuity condition at the TS (at point $\varrho = 1$). Therefore, the GCR energy distribution inside of the HS is defined in a given approximation by the non-modulated GCR spectrum N_0 . Inside the supersonic solar wind ($\varrho < 1$), the particle density is described by the function $N_0(\xi)$, where the variable ξ is defined by Equation 11, and in the heliosheath the GCR density is described by the quantity $N_0(\xi_1)$, where the variable ξ_1 is defined by Equation 7.

The non-modulated GCR spectrum $N_0(\eta)$ in the local IS is here defined in the form (Fedorov, 2015)

$$N_0(\eta) = q_0 \eta^{-\beta} (1 + \eta^2)^{(\beta-\gamma)/2}, \quad (12)$$

where q_0 is a constant that can be computed from the GCR energy density in the IS, for example. A similar form of this spectrum was used in several articles (Goldstein, Ramaty, and Fisk, 1970; Urch and Gleeson, 1972; Dorman *et al.*, 1983; Perko, 1987; Ptuskin *et al.*, 1997; Kolesnik and Shakhov, 2012). According to this formula, the ultra-relativistic particle spectrum ($\eta \gg 1$) is a power law with index γ , which is equal to 4.7 (Perko, 1987; Ptuskin *et al.*, 1997; Webber and McDonald, 2013). In the non-relativistic range ($\eta \ll 1$), the spectrum can be expressed as $N_0(\eta) \propto \eta^\beta$. Using the GCR energy distribution measured by *Voyager 1* in the low-energy range, we obtain $\beta = 1.34$. For these values of the parameters β and γ , the CR spectrum (Equation 12) is in accordance with the *Voyager 1* observations, when the spacecraft left the HS boundary in August 2012 (Webber and McDonald, 2013; Webber, Hiegbie, and McDonald, 2013; Potgieter, 2014; Bisschoff and Potgieter, 2015).

2.1. GCR Spatial Distribution

To determine the GCR energy-spatial distribution inside the HS, we require the values of the CR modulation parameters in both the SW (Equation 9) and in the heliosheath (Equation 5). We applied the data of the GCR intensity modulation provided by Potgieter and Strauss (2013). They specified for protons of kinetic energy 500 MeV that the ratio of GCR intensity at 1 AU to the value of the non-modulated intensity is equal to 0.27. To this value of the CR modulation for 500 MeV protons, the next set of parameters corresponds, for example: $\mu_0 = 1$, $\mu_{01} = 1.8$, $\lambda = 1$, and $\alpha = 2$. The calculated relative GCR intensities at 1 AU for this set are in accordance with the observed data in a proton energy range of 100 MeV up to 100 GeV (Potgieter and Strauss, 2013).

Figure 1a shows the calculated density (Equations 6, 10) for the above set of parameters. The GCR density is normalized to the GCR density in the IS $N_0(\eta)$ (Equation 12). The coordinate $\varrho = 1$ corresponds to the TS, and the heliopause is located at $\varrho = 1.5$. The values of the kinetic energy are indicated near the corresponding curves. The GCR density of a given energy monotonically increases when the heliocentric distance increases up to the heliopause. When the particle energy is enhanced, the transport path increases and the modulation of the GCR intensity inside the HS decreases. Note that under the approximation considered, the GCR intensity outside the HS ($\varrho > 1.5$) is independent of the spatial coordinates, so that the relative particle density there is equal to unity (Figure 1a).

Figure 1b shows the same dependence, but for $\alpha = 8$; this value corresponds to a rapid decrease in SW velocity with increase in coordinate, *i.e.* $u \propto \varrho^{-8}$ for $\varrho \in \{1, \varrho_1\}$. Note here

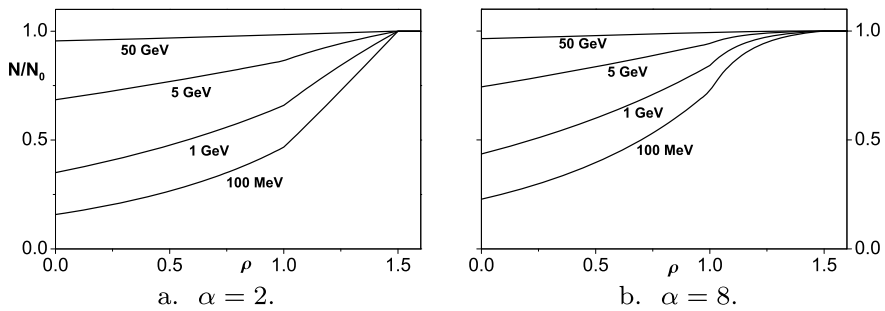


Figure 1 Dependence of the relative GCR density on the heliocentric coordinate for several particle energies and parameters $\mu_0 = 1$, $\mu_{01} = 1.8$, and $\lambda = 1$.

that such a quick decrease in SW velocity is only a model case in the current idealized spherical HS, because in the real HS, the SW plasma can escape into the tail of the heliosheath. (Nevertheless, as follows, the shape of the particle distribution only weakly depends on the value of α .) It is worth noting that numerical solutions of the CR transport equation were obtained for various SW velocity profiles in the heliosheath by Langner *et al.* (2006a, 2006b). The strong decrease in SW velocity in the nose region of the heliosphere ($u = u_0/r^8$) is necessitated by the fact that the SW velocity must become zero when the heliopause is reached, when the SW velocity in the heliosheath decreases rapidly, the relative GCR density converges more quickly to unity as the spatial coordinate increases, and curves that represent $N(\varrho)$ in the range of $1 < \varrho < \varrho_1$ assume a convex shape (Figure 1b).

2.2. GCR Streaming

The calculated GCR density enables estimating the particle streaming at a given energy. For this, the transport equation is rewritten to the form (Gleeson and Webb, 1978; Dorman *et al.*, 1983)

$$\frac{1}{r^2} \frac{\partial}{\partial r} r^2 j + \frac{1}{p^2} \frac{\partial}{\partial p} p^2 j_p = 0, \tag{13}$$

where j is the CR streaming (Equation 3), and j_p is the particle streaming in the momentum space: $j_p = (up/3)(\partial N/\partial r)$. Integrating Equation 13 over the variable r , we obtain

$$j = -\frac{1}{3p^2 r^2} \frac{\partial}{\partial p} p^3 \int_0^r dr r^2 u(r) \frac{\partial N}{\partial r}. \tag{14}$$

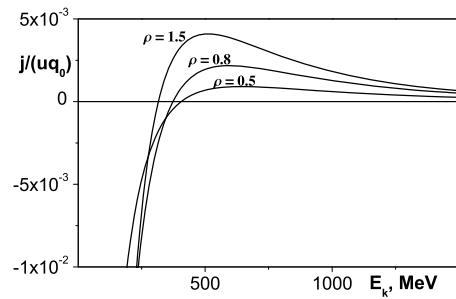
We recall here that the SW velocity u is independent of the coordinate $r < r_0$ ($\varrho < 1$), and it is proportional to $r^{-\alpha}$ in the heliosheath, $r_0 < r < r_1$, (*i.e.* $1 < \varrho < \varrho_1$).

Supersonic Solar Wind From Equation 14, it follows for the SW region that (in variables ϱ, η)

$$j(\varrho, \eta) = -\frac{u_0}{3\eta^2} \left\{ \frac{\partial}{\partial \eta} \eta^3 N(\varrho, \eta) - \frac{2}{\varrho^2} \int_0^\varrho d\varrho \varrho \frac{\partial}{\partial \eta} \eta^3 N(\varrho, \eta) \right\}, \tag{15}$$

where the GCR density $N(\varrho, \eta)$ is determined by Equations 10 and 11.

Figure 2 Energy dependence of the particle streaming for several heliocentric distances and parameters $\mu_0 = 1$, $\mu_{01} = 1.8$, $\lambda = 1$, and $\alpha = 2$.



Heliosheath In the heliosheath ($1 < \varrho < \varrho_1$), the SW velocity is determined by Equation 1, and the GCR streaming is

$$j(\varrho, \eta) = \frac{j(1, \eta)}{\varrho^2} - \frac{u_0}{3\sigma\eta^2} \left\{ \frac{1}{\varrho^\alpha} \frac{\partial}{\partial \eta} \eta^3 N(\varrho, \eta) - \frac{1}{\varrho^2} \frac{\partial}{\partial \eta} \eta^3 N(1, \eta) + \frac{\alpha - 2}{\varrho^2} \int_1^\varrho d\varrho \varrho^{1-\alpha} \frac{\partial}{\partial \eta} \eta^3 N(\varrho, \eta) \right\}, \quad (16)$$

where $N(1, \eta)$, $j(1, \eta)$ are the GCR density at the TS and the GCR streaming, correspondingly. The density $N(\varrho, \eta)$ on the right-hand side of Equation 16 satisfies Equations 6 and 7.

Interstellar Space In the IS ($\varrho > \varrho_1$), the particle streaming changes in inverse proportional to the square of the heliocentric distance,

$$j(\varrho, \eta) = j(\varrho_1, \eta) \frac{\varrho_1^2}{\varrho^2}, \quad (17)$$

where $j(\varrho_1, \eta)$ is the particle streaming at the heliopause.

The GCR streaming is shown in Figure 2, where the dependence of the dimensionless quantity $j/(u_0 q_0)$ of the particle energy is shown. Values of the parameters are $\alpha = 2$, $\mu_0 = 1$, $\mu_{01} = 1.8$, and $\lambda = 1$, and dimensionless coordinates are shown near to the corresponding curves. The GCR streaming of low particle energies is negative, *i.e.* directed toward the Sun, in contrast to the streaming of high GCR energies, which is positive (directed out of the HS). The CR streaming sign changes at values of the proton kinetic energy of about 300–400 MeV depending on the coordinate. After a maximum, the value of the GCR streaming monotonically decreases as the particle energy increases.

2.3. Total GCR Energy Streaming

It is well known that the solar wind does work on the galactic cosmic-ray particles in pushing outward against the cosmic-ray pressure gradient (Jokipii and Parker, 1967, 1976). In their interaction with moving magnetic inhomogeneities, galactic cosmic rays acquire an amount of energy (in unit volume per unit time) that is proportional to the SW velocity and CR density gradient (Gleeson and Webb, 1978; Dorman *et al.*, 1983). In the steady state, the entire energy transferred to the galactic CR particles by SW plasma is carried away from the modulation region by the CR energy streaming. The GCR energy streaming [$J_E(r)$] of particles of energy E follows from (Equation 14), namely

$$J_E(r) = \int_0^\infty dp p^2 E j(r, p) = \frac{1}{3r^2} \int_0^\infty dp p^3 v \int_0^r dr r^2 u(r) \frac{\partial N}{\partial r}, \quad (18)$$

where v is the particle velocity. As a result, we obtain in dimensionless variables the GCR energy streaming in the region of the *supersonic solar wind* ($\varrho < 1$),

$$J_E(\varrho) = \frac{m^4 c^5 u_0}{3} \int_0^\infty d\eta \frac{\eta^4}{\sqrt{1 + \eta^2}} \times \left\{ N(\varrho, \eta) - \frac{2}{\varrho^2} \int_0^\varrho d\varrho \varrho N(\varrho, \eta) \right\}, \tag{19}$$

and in the *heliosheath* ($1 < \varrho < \varrho_1$),

$$J_E(\varrho) = \frac{J_E(1)}{\varrho^2} + \frac{m^4 c^5 u_0}{3\sigma \varrho^2} \int_0^\infty d\eta \frac{\eta^4}{\sqrt{1 + \eta^2}} \left\{ \varrho^{2-\alpha} N(\varrho, \eta) - N(1, \eta) + (\alpha - 2) \int_1^\varrho d\varrho \varrho^{1-\alpha} N(\varrho, \eta) \right\}. \tag{20}$$

Here $J_E(1)$ is the GCR energy streaming on the TS (at $\varrho = 1$).

After the GCRs are scattered by static inhomogeneities of galactic magnetic fields, the fast charged particles do not change their energy in the IS, and the CR energy streaming outside the HS boundary changes proportional to ϱ^{-2} . Therefore, in the space region $\varrho > \varrho_1$, $J_E(\varrho) = J_E(\varrho_1)(\varrho_1^2/\varrho^2)$, where $J_E(\varrho_1)$ is the GCR energy streaming at the heliopause.

In general, the charged-particle energy streaming out of a given volume is determined by the amount of energy that the moving plasma in this volume gives to the fast particles. The amount of energy that the GCR gains in the interplanetary space depends on both the SW velocity [u] and the density of the GCR energy in the IS [w_0]. It is useful to write the energy streaming in the form

$$J_E(\varrho) = u_0 w_0 \Gamma(\varrho), \tag{21}$$

where $\Gamma(\varrho)$ is a dimensionless quantity. Using the GCR energy distribution from Equation 12 outside the HS, we obtain

$$w_0 = m^4 c^5 q_0 \int_0^\infty d\eta \eta^{2-\beta} (1 + \eta^2)^{\frac{\beta-\gamma+1}{2}}. \tag{22}$$

This expression enables calculating the parameter q_0 occurring in Equation 12 when the GCR streaming in interplanetary space is known, namely,

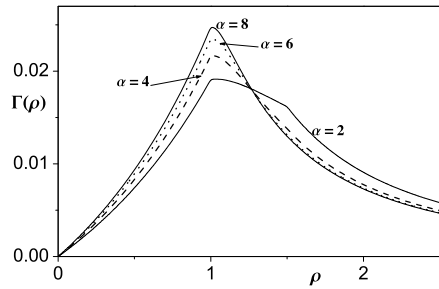
$$q_0 = 0.64 \frac{w_0}{m^4 c^5} \tag{23}$$

for parameters $\beta = 1.34$ and $\gamma = 4.7$.

Figure 3 displays the spatial dependence of $\Gamma(\varrho)$. Numbers near the curves correspond to values of α characterizing the change of SW velocity in Equation 1 in the heliosheath. The following parameters were used: $\mu_0 = 1$, $\mu_{01} = 1.8$, and $\lambda = 1$. The compression coefficient is $\sigma = 3$ on the TS, which is located at a distance $\varrho = 1$, and the heliopause is at $\varrho_1 = 1.5$. The GCR energy streaming in the SW ($\varrho < 1$) increases up to a maximum at the TS.

In the heliosheath ($1 < \varrho < \varrho_1$), the GCR energy streaming decreases with distance from the Sun. Nevertheless, the value of $J_E(\varrho)$ in the heliosheath changes more slowly than ϱ^{-2} over larger distances because in the heliosheath the SW energy is transferred to the GCR. Regardless of the decrease in GCR energy streaming $J_E(\varrho)$ in the heliosheath, the GCR

Figure 3 Particle energy streaming $\Gamma = J_E/u_0w_0$ dependence on dimensionless heliocentric distance.



energy streaming across a sphere of given radius continues to increase with distance, and it reaches a maximum at the heliopause ($\varrho = \varrho_1$). The SW velocity in the heliosheath is lower; therefore, the energy that the solar wind transfers to the GCR decreases. In the IS ($\varrho > 1.5$), the GCR energy streaming $J_E(\varrho)$ changes in inverse proportional to the square of the heliocentric distance, and the GCR energy streaming across a given sphere remains constant.

Energy Streaming Across the Heliosphere Boundary Now we estimate the GCR energy streaming across the surface of the heliopause. The GCR energy density w_0 in the local IS is about 1 eV cm^{-3} . We compare the GCR energy streaming across the heliopause (at 120 AU) with the energy streaming of the SW plasma across a sphere of radius 1 AU: when we set the cosmic plasma density at 1 AU $n_{p1} = 6 \text{ cm}^{-3}$, and the SW velocity $u_0 = 4 \times 10^7 \text{ cm sec}^{-1}$, then the density of plasma kinetic energy is $w_{p1} = 5 \times 10^3 \text{ eV cm}^{-3}$. When $J_{E_{p1}}$ denotes the density of plasma energy streaming, the ratio of the GCR energy streaming across the heliopause to the energy streaming of the SW across the sphere at 1 AU is

$$\frac{J_E(120 \text{ AU})120^2}{J_{E_{p1}}(1 \text{ AU})1^2} = \Gamma(\varrho_1) \frac{w_0}{w_{p1}} \left(\frac{120}{1} \right)^2 = 2.88\Gamma(\varrho_1). \quad (24)$$

This ratio is proportional to the value of Γ at the heliospheric boundary. The value of Γ was calculated for parameters $\mu_0 = 1$, $\mu_{01} = 1.8$, and $\lambda = 1$. The maximum GCR energy streaming across the heliopause is achieved for the minimum value of α ($\alpha = 2$). At this point, $\Gamma(1.5) = 0.016$, and the GCR energy streaming across the heliopause means that 4.6% of the SW plasma energy streams across a sphere of radius 1 AU. For $\alpha = 8$, we obtain $\Gamma(1.5) = 0.013$. In this case, the ratio of the energy streaming in Equation 24 is equal to 0.037, and the GCR particles gain 3.7% of the SW energy. The transfer of the SW energy to the GCR occurs throughout the HS volume, and it depends on both the hydrodynamic velocity of the plasma and the value of the radial gradient of the GCR intensity (Dorman *et al.*, 1983). Note that the GCR energy streaming across the spherical boundary of the HS, when the diffusion coefficient is energy independent, was estimated by Fedorov (2015).

3. GCR Distribution in the Heliosphere

In August 2012, the probe *Voyager 1* reached the surface that separates the solar and interstellar plasma at a heliocentric distance of 122 AU. Near the heliopause, this probe detected a sudden increase in GCR intensity and a simultaneous decrease in the flux of GCR, which is of heliospheric origin (Krimigis *et al.*, 2013; Stone *et al.*, 2013; Kota and Jokipii, 2014).

According to the *Voyager 1* observations, the magnetic field outside the heliopause is parallel with the surface of the heliopause and nearly parallel to the direction of the solar (spiral) field inside the heliopause (Burlaga, Ness, and Stone, 2013). According to the quasi-linear theory, a low level of turbulence in the IS should result in a very large diffusion coefficient parallel to the magnetic field and a very small diffusion coefficient in the perpendicular direction. The model calculations with extremely small cross-field transport in the IS resulted in markedly sharp increases in the GCR streaming at the heliopause. The resulting large gradient in cosmic-ray intensity near the heliopause is in qualitative agreement with *Voyager 1* observations (Kota and Jokipii, 2014; Guo and Florinski, 2014; Zhang, Luo, and Pogorelov, 2015). This means that the radial transport of GCR is hindered in this region of space, and as a consequence the cosmic-ray gradient can greatly exceed its typical values inside the HS. These sudden changes took place within a few weeks, which corresponds to spatial scales significantly smaller than 1 AU (Krimigis *et al.*, 2013; Stone *et al.*, 2013; Kota and Jokipii, 2014). After the short-time rapid increase in GCR intensity in 2012, the intensity detected by *Voyager 1* settled at a nearly constant level. This absence of an observable gradient of the GCR intensity suggests that in the last few years, *Voyager 1* was already located outside the HS, and the particle energy distribution (from about 1 MeV) is coincident with the CR spectrum in the local IS. A possible explanation of the rapid GCR intensity increase near the heliopause was discussed in several articles (Kota and Jokipii, 2014; Guo and Florinski, 2014; Zhang, Luo, and Pogorelov, 2015). They stated that owing to the low turbulence level in the IS, the perpendicular CR diffusion coefficient (with respect to the magnetic field) becomes small, and the CR transport across the HS surface is impeded.

These facts can be included into our greatly idealized model of isotropic diffusion in the spherical HS by the following approach. A perpendicular diffusion plays an important role at the heliopause, where this is the only mechanism that enables the transverse motion of particles (Guo and Florinski, 2014). Because of the low value of the perpendicular mean free path of GCR particles, we can say that particle transport across the heliopause is reduced.

Let the region surrounding the HS, in which the transport of fast charged particles becomes reduced, be situated in some region $\varrho_1 < \varrho < \varrho_2$, and let the quantity $\kappa_i(\varrho, \eta)$ denote the CR diffusion coefficient in some regions of the IS ($\varrho > \varrho_1$). Far away from the HS ($\varrho > \varrho_2$), the value of κ_i considerably exceeds the CR diffusion coefficient [κ] in the HS: $\kappa_i \gg \kappa$. In contrast to this, in the region $\varrho_1 < \varrho < \varrho_2$ $\kappa_i \ll \kappa$. The CR scattering in IS occurs at static magnetic-field inhomogeneities, and the CR streaming is proportional only to the gradient of particle density:

$$j(\varrho, \eta) = -\kappa_i \frac{\partial N(\varrho, \eta)}{\partial \varrho}. \quad (25)$$

Therefore, the CR density in the IS ($\varrho > \varrho_1$) is determined by $N_0(\eta)$ outside the HS and by the CR streaming $j(\varrho_1, \eta)$ across the HS surface, *i.e.*

$$N(\varrho, \eta) = N_0(\eta) + r_0 \varrho_1^2 j(\varrho_1, \eta) \int_{\varrho}^{\infty} \frac{d\varrho}{\varrho^2 \kappa_i(\varrho, \eta)}. \quad (26)$$

For $\varrho \gg \varrho_1$, the contribution of the second term becomes negligible, and the GCR density from Equation 26 tends to $N_0(\eta)$. The most essential contribution to the integral in Equation 26 enters the region of space near the heliopause, which is characterized by a rather low value of the particle transport path.

The direction of particle streaming across the HS surface [$j(\varrho_1, \eta)$] depends on the particle energy. The high-energy particle streaming is directed out of the HS (see Figure 2), thus the particle density on the heliopause exceeds the CR density far away from the solar system. Unlike this, the low-energy particle streaming is negative, and according to Equation 26, the GCR density near the HS is lower than the value of $N_0(\eta)$ at large distances. In the region $\varrho > \varrho_1$, the intensity of high-energy GCR therefore decreases, while the intensity of low-energy GCS increases with increasing distance from the HS.

3.1. GCR Transport Near the Heliopause

Near the heliopause ($\varrho_1 < \varrho < \varrho_2$), the CR transport is weak and the diffusion coefficient has a remarkably lower value than in the HS. The characteristic dimension of this region $\{\varrho_1, \varrho_2\}$ is about one AU. Let κ_2 be the CR diffusion coefficient in this spherical layer and the inequality $\kappa_2 \ll \kappa$ holds, where κ is the diffusion coefficient in the SW. Moreover, let

$$\kappa_2(\eta) = \kappa_{02}\eta^\lambda \quad (27)$$

with the same power λ as inside the HS.

3.1.1. Local Interstellar Space

Let the particle transport in the IS ($r > r_2$) be characterized by the diffusion coefficient $\kappa_i \equiv \kappa_3(\eta)$, $\kappa_3 \gg \kappa$, and

$$\kappa_3(\eta) = \kappa_{03}\eta^\lambda. \quad (28)$$

Then from Equation 26, we obtain in the region $\varrho_1 < \varrho < \varrho_2$ a GCR density

$$N(\varrho, \eta) = N_0(\eta) + r_0\varrho_1^2 j(\varrho_1, \eta)\eta^{-\lambda} \left\{ \frac{1}{\kappa_{02}} \left(\frac{1}{\varrho} - \frac{1}{\varrho_2} \right) + \frac{1}{\kappa_{03}\varrho_2} \right\}, \quad (29)$$

and for $\varrho > \varrho_2$

$$N(\varrho, \eta) = N_0(\eta) + \frac{r_0\varrho_1^2}{\kappa_{03}\varrho} j(\varrho_1, \eta)\eta^{-\lambda}. \quad (30)$$

3.1.2. Heliopause

The GCR density at the heliopause (at point $\varrho = \varrho_1$) follows from Equation 29:

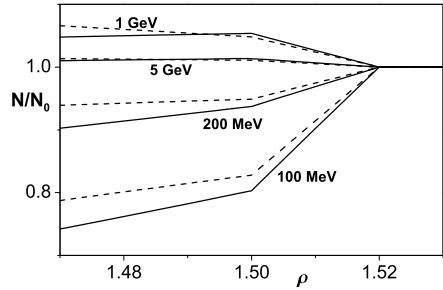
$$\begin{aligned} \Psi_1(\eta) &\equiv N(\varrho_1, \eta) \\ &= N_0(\eta) + r_0\varrho_1^2 j(\varrho_1, \eta)\eta^{-\lambda} \left\{ \frac{1}{\kappa_{02}} \left(\frac{1}{\varrho_1} - \frac{1}{\varrho_2} \right) + \frac{1}{\kappa_{03}\varrho_2} \right\}. \end{aligned} \quad (31)$$

3.1.3. Heliosheath

Using both the assumption of zero streaming of the GCR on the heliopause (Equation 4) and the boundary condition (Equation 31) at ϱ_1 , we obtain that $N(\varrho, \eta) = \Psi_1(\xi_1)$ for the GCR density in the region $1 < \varrho < \varrho_1$, where the variable ξ_1 is defined in Equation 7. The density is represented by the sum

$$N(\varrho, \eta) = \Psi_1(\xi_1) + N_1(\varrho, \eta). \quad (32)$$

Figure 4 GCR density near the HS boundary. Parameter $\alpha = 2$ (solid curves), and $\alpha = 8$ (dashed curves).



The function $\Psi_1(\xi_1)$ corresponds to zero CR streaming, and it satisfies the boundary condition in Equation 31; the quantity $N_1(\varrho, \eta)$ satisfies the zero boundary condition at the heliopause:

$$N_1(\varrho_1, \eta) = 0. \tag{33}$$

The GCR streaming in the heliosheath expressed by Equation 4 can be rewritten in the form

$$\frac{\partial N_1(\varrho, \eta)}{\partial \varrho} + \frac{\eta \mu_1(\eta)}{3\varrho^\alpha} \frac{\partial N_1(\varrho, \eta)}{\partial \eta} = \Phi_1(\varrho, \eta), \tag{34}$$

$$\Phi_1(\varrho, \eta) = -\frac{\sigma \mu_1(\eta)}{u_0} j(\varrho, \eta),$$

and the modulation parameter $\mu_1(\eta)$ is defined in Equation 5. Equation 34 differs from the zero streaming in Equation 4 by the presence of the right-hand side, which is proportional to the GCR streaming (Equation 16) in the heliosheath. The solution of Equation 34 that satisfies the zero boundary condition on the sphere of radius ϱ_1 , (Equation 33), reads

$$N_1(\varrho, \eta) = \int_{\varrho_1}^{\varrho} d\rho \Phi_1(\rho, \chi_1), \tag{35}$$

$$\chi_1 = \left[\eta^\lambda + \frac{\mu_{01}\lambda}{3(\alpha - 1)} (\varrho^{1-\alpha} - \rho^{1-\alpha}) \right]^{1/\lambda}.$$

Therefore, the GCR density in the heliosheath (Equation 32) takes the final form

$$N(\varrho, \eta) = \Psi_1(\xi_1) + \int_{\varrho_1}^{\varrho} d\rho \Phi_1(\rho, \chi_1). \tag{36}$$

The GCR density dependence on the heliocentric distance near the HS boundary given by Equations 29–36 is shown in Figure 4. The density is normalized to the quantity $N_0(\eta)$, and particle kinetic energies are marked near the corresponding curves. The calculations were performed for parameters $\varrho_1 = 1.5$, $\varrho_2 = 1.52$, $\mu_0 = 1.2$, $\mu_{01} = 1.8$, and $\lambda = 1$. In the thin spherical layer $[\varrho_1 < \varrho < \varrho_2]$ surrounding, the HS the particle transfer is weak and the diffusion coefficient is therefore two orders smaller than inside the HS. In the local IS $[\varrho > \varrho_2]$, the transport path sufficiently exceeds the corresponding value in the SW ($\kappa_3 \doteq 10^3 \kappa$). It is seen that in the relatively thin transition layer ($1.5 < \varrho < 1.52$), the intensity gradient considerably exceeds the corresponding value inside the HS. The radial gradient for low-energy particles is positive, and the GCR intensity increases for increasing distances. On the other hand, the radial gradient for higher particle energies in the region $\varrho > 1.5$ becomes

negative, such that the GCR density at the HS boundary exceeds the GCR density in the local IS. Beyond the HS boundary, the GCR density approaches the value characteristic for the IS and its relative value tends to unity. Note that owing to the long transport path in IS, the GCR density in the region $\varrho > 1.52$ becomes independent of the coordinate.

3.2. GCR Spatial Distribution in the Solar Wind

When we set the dimensionless distance $\varrho = 1$ in Equation 36, we found the GCR density at the TS,

$$\begin{aligned}\Psi(\eta) \equiv N(1, \eta) &= \Psi_1(\xi_2) + \int_{\varrho_1}^1 d\rho \Phi_1(\rho, \chi_2), \\ \xi_2 &= \left[\eta^\lambda + \frac{\mu_{01}\lambda}{3(\alpha-1)} (1 - \varrho_1^{1-\alpha}) \right]^{1/\lambda}, \\ \chi_2 &= \left[\eta^\lambda + \frac{\mu_{01}\lambda}{3(\alpha-1)} (1 - \rho^{1-\alpha}) \right]^{1/\lambda}.\end{aligned}\quad (37)$$

The GCR density in the SW ($\varrho < 1$) can be written in the form

$$N(\varrho, \eta) = \Psi(\xi) + N_1(\varrho, \eta), \quad (38)$$

where the variable ξ is defined in Equation 11. The GCR streaming corresponding to the first term in Equation 38 is equal to zero, and the function Ψ satisfies the boundary condition (Equation 37) at $\varrho = 1$. The GCR streaming in the SW has the form given in Equation 8. When we introduce the expression of Equation 38 into this relation, we therefore obtain

$$\begin{aligned}\frac{\partial N_1(\varrho, \eta)}{\partial \varrho} + \frac{\eta \mu(\eta)}{3} \frac{\partial N_1(\varrho, \eta)}{\partial \eta} &= \Phi(\varrho, \eta), \\ \Phi(\varrho, \eta) &= -\frac{\mu(\eta)}{u_0} j(\varrho, \eta).\end{aligned}\quad (39)$$

Here parameter $\mu(\eta)$ is determined in Equation 9, and the GCR streaming in the SW [$j(\varrho, \eta)$] is described by Equation 15. The right-hand side of Equation 39 is the defined function of coordinate and momentum, and function $N_1(\varrho, \eta)$ satisfies the condition at the TS ($\varrho = 1$), namely, $N_1(1, \eta) = 0$. The solution of Equation 39 that fulfills the last condition is

$$N_1(\varrho, \eta) = \int_1^\varrho d\rho \Phi(\rho, \chi), \quad \chi = \left[\eta^\lambda + \frac{\mu_0\lambda}{3} (\rho - \varrho) \right]^{1/\lambda}. \quad (40)$$

So, the GCR density in the solar wind acquires the form

$$N(\varrho, \eta) = \Psi(\xi) + \int_1^\varrho d\rho \Phi(\rho, \chi), \quad (41)$$

where the function Ψ is determined in Equation 37. Therefore, the GCR density in the SW ($\varrho < 1$) is described by Equation 41, in the heliosheath ($1 < \varrho < \varrho_1$) by Equation 36, and in IS ($\varrho > \varrho_1$) by Equations 29–30.

The GCR spatial distribution is shown in Figure 5. The parameters have the same values as in Figure 4. The GCR density is normalized to the value $N_0(\eta)$ (Equation 12). The GCR

Figure 5 Spatial distribution of the GCR. The particle kinetic energy is indicated near the curves. Parameter $\alpha = 2$ (solid curves), and $\alpha = 8$ (dashed curves).

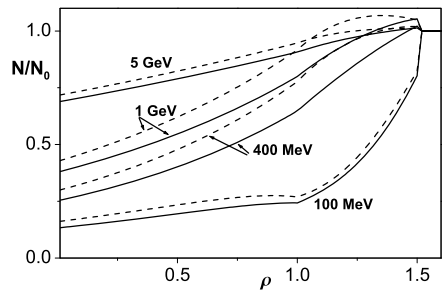
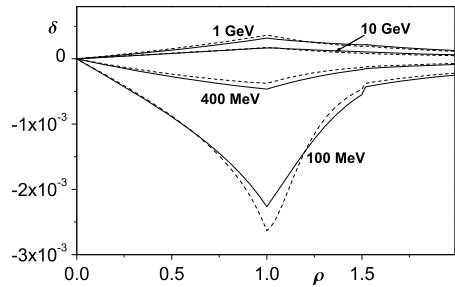


Figure 6 Spatial dependence of the anisotropy in the GCR angular distribution for various particle kinetic energies. Parameter $\alpha = 2$ (solid curves), and $\alpha = 8$ (dashed curves).



density of very low energies (see the curve for 100 MeV) monotonically increases with distance. The intensity of high-energy particles (1 GeV) is characterized by the maximum near the heliopause ($\rho = 1.5$). After this maximum, the intensity rapidly decreases and tends to the value of N_0 in the local IS. Of course, the radial gradient has a high value in the thin transient layer surrounding the HS. The gradient in this layer is rather dominant, especially for low-energy particles. These facts correspond to data of *Voyager 1* (Krimigis *et al.*, 2013; Stone *et al.*, 2013; Webber, Hiegbie, and McDonald, 2013; Kota and Jokipii, 2014).

GCR Anisotropy The anisotropy in the particle distribution is proportional to the particle streaming. Figure 6 demonstrates the spatial dependence of the GCR anisotropy

$$\delta(\rho, \eta) = 3j/vN$$

for several energies. The parameters are the same as in previous figures. The absolute value of the anisotropy has a maximum at $\rho = 1$. This is positive for high energies (the curves for energy of 1 GeV and 10 GeV). Thus the streaming of these particles is directed away from the Sun. In contrast, the anisotropy of lower-energy particles is negative. Note the rapid change in the GCR anisotropy value near the heliopause (especially for low-energy particles), which is subject to the presence of the transition region around the HS, where particles are strongly scattered.

3.3. GCR Energy Spectra

The particle intensity is proportional to the particle density and is in general defined by the relation $I(r, p) = p^2 N(r, p)/(4\pi)$. Figure 7 shows the dependence of the quantity $\eta^2 N(\rho, \eta)/q_0$ (which is proportional to the intensity) on the particle kinetic energy. The quantity q_0 is defined in Equation 23. The parameters have the same values as in previous figures, and, the numbers near curves indicate the dimensionless heliocentric distances $\rho = r/r_0$.

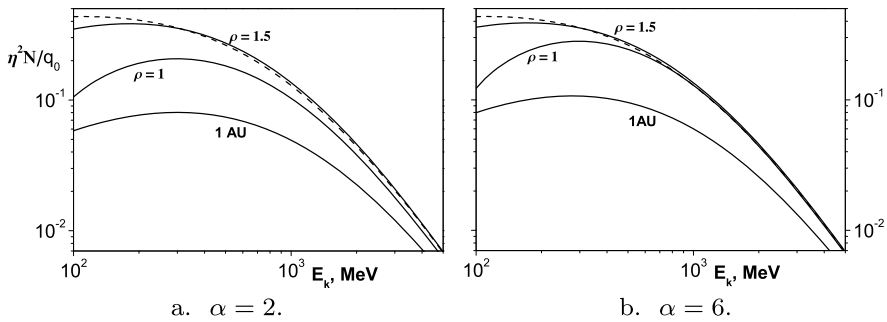


Figure 7 GCR energy spectra for two heliocentric distances, $\rho = 1$ and 1.5. The *dashed curve* shows the energy spectrum out of the solar system, the *lowest curve* corresponds to the energy spectrum at Earth's orbit.

The GCR spectrum outside the solar system [$N_0(\eta)$] (Equation 12) is represented by the dashed curve; in good agreement with the *Voyager 1* observations when the probe left the HS (Potgieter, 2013; Webber and McDonald, 2013). The GCR intensity and its energy spectrum outside the Galaxy can certainly differ significantly from their values in the local IS. The curve for $\rho = 1.5$ illustrates the GCR intensity on the heliopause, and the curve for $\rho = 1$ corresponds to the TS. The lowest curve corresponds to the GCR energy spectrum at Earth's orbit. The modulation depth of the GCR intensity increases toward smaller radial distances, and the maximum of the energy distribution shifts toward the region of high energies. The relative reduction of GCRs inside the HS is larger at low GCR energies because the diffusion coefficient decreases toward lower energies. In the low-energy range (lower than ≈ 400 MeV), the GCR flux at the heliopause is lower than in the IS. At higher energies, the spectrum of GCRs at the heliopause and in the IS are very similar, with a slight excess at the heliopause. This is in agreement with the spatial variations in GCR densities shown in Figures 4 and 5. In fact, the high-energy particle density is maximum at the heliopause (the curves for the kinetic energy of 1 GeV and 5 GeV in Figures 4 and 5), and their density decreases for larger distances.

Figure 7b shows energy spectra for the parameter $\alpha = 6$ when the SW velocity falls faster with increasing radial distances. In this case, the GCR energy distribution in the range $E_k \geq 800$ MeV at the TS differs slightly from the GCR spectrum in the local IS (the dashed curve). Therefore, the GCR modulation in this energy range is weak at the heliopause, which is caused by a rapid decline in SW velocity in the spatial range of $1 < \rho < 1.5$.

4. Discussion and Conclusions

The present article was devoted to the GCR distribution in the heliosphere. This region consists of the supersonic solar wind surrounded by the termination shock, the heliosheath, and the heliopause, which separates the heliosphere from the local interstellar space. The analytical calculations were performed by a perturbative method using the anisotropy in the CR angular distribution as a smallness parameter, and by fixing the form of the non-modulated GCR energy spectrum in the local interstellar space that is commonly used in the literature (see Section 2). All calculations were made for the power-law dependence of the solar-wind velocity on the heliocentric distance in the heliosheath (proportional to $r^{-\alpha}$). However, differences in CR distribution for various values of α are not very notable.

The well-known force-field solutions were investigated as the initial point. It is well known that the force-field solution for the spherical symmetric heliosphere shows good agreement with numerical simulations for particles with an energy range above 150 MeV (Gleeson and Urch, 1973; Caballero-Lopez and Moraal, 2004; Moraal, 2013); this makes it suitable for describing the energy-spatial distribution of the GCR in the inner heliosphere. Comparison of these solutions with analytical solutions of the transport equation assuming an energy-independent diffusion coefficient indicates that the force-field solution is a good approximation for various dependences of the solar-wind velocity $u(r)$ on coordinate (such as a rapidly decreasing solar-wind velocity when $\text{div } \mathbf{u} < 0$).

We were able to ascertain that the next iteration (with respect to the well-known force-field solution) using a weak GCR anisotropy considerably improves the agreement between approximate and exact solutions of the CR transport equation even if the modulation parameter $\mu \geq 1$. Nevertheless, the application of a given perturbative method is limited for low-energy particles because the diffusion coefficient decreases for lower energies of the particles, and therefore the modulation parameter increases. In the present article the propagation of particles with energies above 100 MeV was considered. It should be noted, however, that the validity of the approximate solution of CR transport equation is dependent upon the type of galactic spectrum and interplanetary conditions (Gleeson and Urch, 1973; Caballero-Lopez and Moraal, 2004).

The cosmic-ray transport has been studied separately in all regions of the heliosphere. It was found that

- the direction of the GCR streaming depends on the particle energy: the high-energy particle streaming is oriented out of the solar system, and the streaming of low-energy particles is directed toward the Sun;
- for a faster decrease of the solar-wind velocity in the heliosheath (when $\alpha = 8$), the relative GCR density converges faster to unity with increasing distances;
- the energy flux of the GCR is directed outward from the heliosphere, so that the bulk of the GCR particles gains energy during their interaction with moving interplanetary field inhomogeneities; the energy of the moving solar-wind plasma is transferred to the GCR throughout the heliosphere, and its magnitude depends on the value of the radial gradient of the GCR intensity;
- the GCR intensity in the local interstellar space that surrounds the heliosheath is dependent on both the value and the direction of the fast particle streaming across the heliospheric surface;
- in accordance with the GCR streaming direction, the density of high-energy particles in interstellar space decreases as the distance from the heliopause increases, and it increases for low-energy particles;
- the GCR density gradient in the transition layer near the heliopause, which is characterized by a low value of the particle transport path, significantly exceeds the gradient inside the heliosphere;
- with decreasing heliocentric distances, the magnitude of the GCR intensity modulation increases and the maximum in the energy distribution is shifted to high energies;
- at low energies, the GCR intensity in the interstellar space exceeds its corresponding value at the heliopause. At the same time, the intensity in the high-energy range near the heliopause is higher than in the remote interstellar region; and finally,
- the sign of the anisotropy in the GCR angular distribution depends on the particle energy, and its absolute value is maximum at the termination shock.

Acknowledgements The authors are grateful to the referee for corrections and useful suggestions. This work was partially supported by the Slovak Research and Development Agency under the contract No. APVV-15-0194, and by SAS, VEGA projects No. 2/0026/16 and 2/0065/17.

Disclosure of Potential Conflicts of Interest The authors declare that they have no conflicts of interest.

References

- Bischoff, D., Potgieter, M.S.: 2015, New local interstellar spectra for protons, Helium and Carbon derived from PAMELA and Voyager 1 observations. *Astrophys. Space Sci.* **361**, 48. DOI.
- Burlaga, L.F., Ness, N.F., Acuna, M.H., Lepping, R.P., Connerney, J.E.P., Stone, E.C., McDonald, F.B.: 2005, Crossing the termination shock into the heliosheath: Magnetic fields. *Science* **309**, 2027. DOI.
- Burlaga, L.F., Ness, N.F., Stone, E.C.: 2013, Magnetic field observations as Voyager 1 entered the heliosheath depletion region. *Science* **341**, 147. DOI.
- Burlaga, L.F., Ness, N.F., Acuna, M.H., Lepping, R.P., Connerney, J.E.P., Richardson, J.D.: 2008, Magnetic fields at the solar wind termination shock. *Nature* **454**, 75. DOI.
- Burlaga, L.F., Ness, N.F., Acuna, M.H., Richardson, J.D., Stone, E., McDonald, F.B.: 2009, Observation of the heliosheath and solar wind near the termination shock by Voyager 2. *Astrophys. J.* **692**, 1125. DOI.
- Caballero-Lopez, R.A., Moraal, H.: 2004, Limitations of the force field equation to describe cosmic ray modulation. *J. Geophys. Res.* **109**, A01101. DOI.
- Cummings, A.C., Stone, E.C., Heikkilä, B.C., Lal, N., Webber, W.R., Johannesson, G., *et al.*: 2015, Voyager 1 observations of galactic cosmic rays in the local interstellar medium: Energy density and ionization rates. In: *Proc. of 34th Int. Cosmic Ray Conf.*, Proceeding Science Server, The Hague, 318.
- Decker, R.B., Krimigis, S.M., Roelof, E.C., Hill, M.E., Armstrong, T.P., Gloeckler, G., *et al.*: 2005, Voyager 1 in the foreshock, termination shock, and heliosheath. *Science* **309**, 2020. DOI.
- Decker, R.B., Krimigis, S.M., Roelof, E.C., Hill, M.E., Armstrong, T.P., Gloeckler, G., *et al.*: 2008, Mediation of the solar wind termination shock by non-thermal ions. *Nature* **454**, 67. DOI.
- Dolginov, A.Z., Toptygin, I.N.: 1966, *Ž. ěksp. Teor. Fiz.* **51**, 1771.
- Dorman, L.I.: 2006, *Cosmic Ray Interactions, Propagation, and Acceleration in Space Plasmas*, Springer, Dordrecht.
- Dorman, L.I., Katz, M.E., Fedorov, Yu.I., Shakhov, B.A.: 1983, Variation of cosmic ray energy in interplanetary space. *Astrophys. Space Sci.* **94**, 43.
- Fedorov, Yu.I.: 2014, Charged particle acceleration in the front of the shock wave bounding supersonic solar wind. *Kinemat. Phys. Celest. Bodies* **30**, 109. DOI.
- Fedorov, Yu.I.: 2015, Modulation of galactic cosmic ray intensity in the turbulent heliosphere. *Kinemat. Phys. Celest. Bodies* **31**, 105. DOI.
- Florinski, V., Pogorelov, N.V.: 2009, Four-dimensional transport of galactic cosmic rays in the outer heliosphere and heliosheath. *Astrophys. J.* **701**, 642. DOI.
- Gleeson, L.J., Axford, W.I.: 1968, Solar modulation of galactic cosmic rays. *Astrophys. J.* **154**, 1011.
- Gleeson, L.J., Urch, I.H.: 1973, A study a force-field equation for the propagation of galactic cosmic rays. *Astrophys. Space Sci.* **25**, 387.
- Gleeson, L.J., Webb, G.M.: 1978, Energy changes of cosmic rays in the interplanetary region. *Astrophys. Space Sci.* **58**, 21.
- Goldstein, M.L., Ramaty, R., Fisk, L.A.: 1970, Interstellar cosmic ray spectra from the non-thermal radio background from 0.4 to 400 MHz. *Phys. Rev. Lett.* **24**, 1193.
- Guo, X., Florinski, V.: 2014, Galactic cosmic-ray modulation near the heliopause. *Astrophys. J.* **793**, 18. DOI.
- Herbst, K., Heber, B., Kopp, A., Sternal, O., Steinhilber, F.: 2012, The local interstellar spectrum beyond the heliopause: What can we learn from Voyager in the inner heliosheath? *Astrophys. J.* **761**, 17. DOI.
- Jokipii, J.R., Parker, E.N.: 1967, Energy changes of cosmic rays in the solar system. *Planet. Space Sci.* **15**, 1375.
- Jokipii, J.R., Parker, E.N.: 1976, On the physical interpretation on the cosmic-ray transport equation. *Astrophys. J.* **208**, 220.
- Kolesnik, Yu.L., Shakhov, B.A.: 2012, Effect of the heliosheath and standing termination shock on galactic cosmic ray propagation in a stationary heliosphere model. *Kinemat. Phys. Celest. Bodies* **28**, 261. DOI.
- Kota, J., Jokipii, J.R.: 2014, Are cosmic rays modulated beyond the heliopause? *Astrophys. J.* **782**, 24. DOI.
- Krimigis, S.M., Decker, R.B., Roelof, E.C., Hill, M.E., Armstrong, T.P., Gloeckler, G., *et al.*: 2013, Search for the exit: Voyager 1 at heliosphere's border with the Galaxy. *Science* **341**, 144. DOI.
- Langner, U.W., Potgieter, M.S., Fichtner, H., Borrmann, T.: 2006a, Effects of different solar wind speed profiles in the heliosheath on the modulation of cosmic-ray protons. *Astrophys. J.* **640**, 1119. DOI.

- Langner, U.W., Potgieter, M.S., Fichtner, H., Borrmann, T.: 2006b, Modulation of anomalous protons: Effects of different solar wind speed profiles in the heliosheath. *J. Geophys. Res.* **111**, A01106. DOI.
- Manuel, R., Ferreira, S.E.S., Potgieter, M.S.: 2014, Time-dependent modulation of cosmic rays in the heliosphere. *Solar Phys.* **289**, 2207. DOI.
- Moraal, H.: 2013, Cosmic ray modulation equations. *Space Sci. Rev.* **176**, 299. DOI.
- Parker, E.N.: 1965, The passage of energetic charged particles through interplanetary space. *Planet. Space Sci.* **13**, 9.
- Perko, J.S.: 1987, Solar modulation of galactic antiprotons. *Astron. Astrophys.* **184**, 119.
- Potgieter, M.S.: 2013, Solar modulation of cosmic rays. *Living Rev. Solar Phys.* **10**, 3. DOI.
- Potgieter, M.S.: 2014, A very local interstellar spectrum for galactic electrons, protons and helium. *Braz. J. Phys.* **44**, 581.
- Potgieter, M.S., Strauss, R.T.: 2013, At what rigidities does the solar modulation of galactic cosmic rays begin? In: Saa, A. (ed.) *Proc. of 33rd Int. Cosmic Ray Conf.*, Springer Server, Rio de Janeiro, 0156.
- Ptuskin, V.S., Volk, H.J., Zirakashvili, V.N., Breitschwerdt, D.: 1997, Transport of relativistic nucleons in a galactic wind driven by cosmic rays. *Astron. Astrophys.* **321**, 434.
- Richardson, J.D., Burlaga, L.F.: 2013, The solar wind in the outer heliosphere and heliosheath. *Space Sci. Rev.* **176**, 217. DOI.
- Richardson, J.D., Stone, E.C.: 2009, The solar wind in the outer heliosphere. *Space Sci. Rev.* **143**, 7. DOI.
- Richardson, J.D., Kasper, J.C., Wang, C., Belcher, J.W., Lazarus, A.J.: 2008, Cool heliosheath plasma and deceleration of the upstream solar wind at the termination shock. *Nature* **454**, 63. DOI.
- Scherer, K., Fichtner, H., Strauss, R.D., Ferreira, S.E.S., Fahr, H.-J.: 2011, On cosmic ray modulation beyond the heliopause: Where is the modulation boundary? *Astrophys. J.* **735**, 128. DOI.
- Schlickeiser, R.: 2002, *Cosmic Ray Astrophysics*, Springer, Berlin.
- Shakhov, B.A., Kolesnik, Yu.L.: 2006, Iterative method for solving boundaryvalue problems in the theory of cosmic ray propagation. *Kinemat. Phys. Celest. Bodies* **22**, 61.
- Stone, E.C., Cummings, A.C., McDonald, F.B., Heikkila, B.C., Lal, N., Webber, W.R.: 2005, Voyager 1 explores the termination shock region and the heliosheath beyond. *Science* **309**, 2017. DOI.
- Stone, E.C., Cummings, A.C., McDonald, F.B., Heikkila, B.C., Lal, N., Webber, W.R.: 2008, An asymmetric solar wind termination shock. *Nature* **454**, 71. DOI.
- Stone, E.C., Cummings, A.C., McDonald, F.B., Heikkila, B.C., Lal, N., Webber, W.R.: 2013, Voyager 1 observes low-energy galactic cosmic rays in a region depleted of heliospheric ions. *Science* **341**, 150. DOI.
- Strauss, R.D., Fichtner, H.: 2014, Cosmic ray anisotropies near the heliopause. *Astron. Astrophys. Lett.* **572**, L3. DOI.
- Urch, I.H., Gleeson, L.J.: 1972, Galactic cosmic ray modulation from 1965 – 1970. *Astrophys. Space Sci.* **17**, 426.
- Webber, W.R., McDonald, F.B.: 2013, Recent Voyager 1 data indicate that on 25 August 2012 at a distance of 121.7 AU from the Sun, sudden and unprecedented intensity changes were observed in anomalous and galactic cosmic rays. *Geophys. Res. Lett.* **40**, 1665. DOI.
- Webber, W.R., Hiegbie, P.R., McDonald, F.B.: 2013, The unfolding of the spectra of low energy galactic cosmic ray H and He nuclei as the Voyager 1 spacecraft exits the region of heliospheric modulation. [arXiv](#).
- Zhang, M., Luo, X., Pogorelov, N.: 2015, Where is the cosmic-ray modulation boundary of the heliosphere? *Phys. Plasmas* **22**, 091501. DOI.